Available online at www.sciencedirect.com

SciVerse ScienceDirect

Ceramics International 38 (2012) 2773–2778

CERAMICS INTERNATIONAL

www.elsevier.com/locate/ceramint

Structural, electrical and magnetic properties of $Co_{0.5}Zn_{0.5}Al_xFe_{2-x}O_4$ ($x = 0$, 0.2, 0.4, 0.6, 0.8 and 1.0) prepared via sol–gel route

Sonal Singhal *, Rimi Sharma, Tsering Namgyal, Sheenu Jauhar, Santosh Bhukal, Japinder Kaur

Department of Chemistry, Panjab University, Chandigarh 160 014, India

Received 4 May 2011; received in revised form 14 November 2011; accepted 16 November 2011
Available online 25 November 2011

Abstract

Nanoparticles of $Co_{0.5}Zn_{0.5}Al_xFe_{2-x}O_4$ ($x = 0$, 0.2, 0.4, 0.6, 0.8 and 1.0) were synthesized by sol–gel method and the influence of Al^{3+} doping on the properties of $Co_{0.5}Zn_{0.5}Fe_2O_4$ was studied. X-ray diffraction studies revealed the formation of single phase spinel type cubical structure having space group Fd-3m. A decreasing trend of the lattice parameter was observed with increasing Al^{3+} concentration due to the smaller ionic radii of Al^{3+} ion as compared to Fe^{3+} ion. TEM was used to characterize the microstructure of the samples and particle size determination, which exhibited the formation of spherical nanoparticles. The particle size was found to be increases up to ~45 nm after annealing the sample at 1000 °C. Electrical resistivity was found to increase with Al^{3+} doping, attributed to the decrease in the number of Fe^{2+}–Fe^{3+} hopping. The activation energy decreased with increasing Al^{3+} ion concentration, indicating the blocking of conduction mechanism between Fe^{3+}–Fe^{2+} ions. The value of saturation magnetization decreased, when Fe^{3+} ions were doped with Al^{3+} ions in $Co_{0.5}Zn_{0.5}Fe_2O_4$; however, the coercivity values increased with increasing Al^{3+} ion content.

Keywords: C. Electrical properties; D. Ferrites; Saturation magnetization; Coercivity; X-ray diffraction

1. Introduction

Spinel ferrites belong to a class of magnetic materials having applications in many fields such as in magnetic devices, microwave devices, electrical devices, disk recording, and ferrofluids. $CoFe_2O_4$ is such a class of ferrite material that has high saturation magnetization, high coercivity, large remenance and high chemical stability due to which it acts as a promising material in high density magnetic recording media [1]. Cobalt ferrite has an inverse spinel structure with Co^{2+} ions in the octahedral (B) sites and Fe^{3+} ions equally distributed between tetrahedral (A) and octahedral (B) sites. Therefore, substitution with various metal cations allows some tunable changes in the properties of these nanoferrites [2–6].

Singhal et al. [7] have reported an unusual behavior of saturation magnetization in Zn substituted cobalt ferrites, $Co_xZn_{1-x}Fe_2O_4$, ($x = 0.0$, 0.2, 0.4, 0.6, 0.8, and 1.0). The saturation magnetization first increases with Zn doping upto $x = 0.4$, and then decreases as the concentration of Zn^{2+} is further increased. This may be due to the weakening of A–B interaction and strengthening of B–B interactions at higher concentration of Zn^{2+} ions. Thanki et al. [8] have prepared $Zn_xCo_{1-x}Fe_{2-x}Al_xO_4$ where $x = 0.0 \leq x \leq 0.9$ and conducted a Mossbauer study which exhibit the existence of two hyperfine fields for $x = 0.0$ and 0.4, and relaxation effects for $x = 0.5$ and 0.6. The samples with $x > 0.6$ exhibit a paramagnetic quadrupole doublet. Alone and Jadhav [9] have prepared $Co_{1-x}Zn_xFe_{2-x}Al_xO_4$ ($x = 0.0 \leq x \leq 0.6$) and reported that Zn^{2+} and Al^{3+} ions have a larger influence on the structural and magnetic properties of cobalt ferrite as compared to Zn^{2+} and Al^{3+} being separately doped in $CoFe_2O_4$ lattice. Zinc substituted cobalt ferrialuminates $Zn_xCo_{1-x}FeAlO_4$ ($x = 0.2$–0.5) synthesized by Vasoya et al. [10] are found to have conducting behavior.

Although a tremendous work has been reported on zinc doped cobalt ferrites, but the simultaneous investigation of the variation of electrical and magnetic properties of Co–Zn nanoferrites with Al^{3+} ions has not been reported earlier. Therefore, in the present investigation, an attempt is made to synthesize $Co_{0.5}Zn_{0.5}Al_xFe_{2-x}O_4$ ($x = 0$–1.0) using sol–gel

* Corresponding author. Tel.: +91 9872118810.
E-mail address: sonal1174@gmail.com (S. Singhal).

0272-8842/$36.00
doi:10.1016/j.ceramint.2011.11.047

method and study the effects of simultaneous substitution of Zn^{2+} and Al^{3+} ions on the electrical and magnetic properties of cobalt nanoferrites.

2. Experimental

2.1. Preparation of $Co_{0.5}Zn_{0.5}Al_xFe_{2-x}O_4$ ($x = 0$, 0.2, 0.4, 0.6, 0.8 and 1.0) nanoferrrites by sol–gel method

Al-substituted Co–Zn nanoferrites, $Co_{0.5}Zn_{0.5}Al_xFe_{2-x}O_4$ ($x = 0$, 0.2, 0.4, 0.6, 0.8 and 1.0) were prepared using the sol–gel method [7]. This method was chosen to obtain homogeneous materials at relatively low temperatures. In this method, the precursor nitrates were accurately weighed in stoichiometric proportion and dissolved separately in minimum amount of distilled water. The solutions were then heated at 80°–90 °C and mixed with constant stirring. Citric acid (in the molar ratio 1:1 to metal cations) was then added followed by ethylene glycol to the nitrates solution. The solution was stirred until gel formation. Then these gels were self ignited until ferrite powder was obtained, which was annealed at 400, 600, 800 and 1000 °C for 2 h for further characterization.

2.2. Physical measurements

The infrared spectra for all the samples were recorded using FT-IR spectrophotometer (Perkin Elmer) using KBr pellets in the range 4000–400 cm^{-1}. TEM images were recorded using Hitachi (H7500) transmission electron microscope, operated at 120 kV. The X-ray diffraction studies were carried out by X-ray diffractometer (Bruker AXS, D8 Advance) with Cu-Kα radiation. The electrical resistivity was measured using a two probe method. The magnetic measurements were made on a vibrating sample magnetometer (VSM) (155, PAR).

3. Results and discussions

3.1. FT-IR characterization

The FT-IR spectroscopy indicates the positions of the ions involved in the crystal lattice through their vibrational modes. The typical IR spectrum of $Co_{0.5}Zn_{0.5}Al_xFe_{2-x}O_4$ with (a) $x = 0.0$, (b) $x = 0.6$ and (c) $x = 1.0$ nanoferrites annealed at 1000 °C, which are shown in Fig. 1, indicates the presence of two fundamental peaks at ~580 cm^{-1} and ~450 cm^{-1}, which correspond to the crystal vibrations of M–O bonds in the ferrites. The frequency band near 580 cm^{-1} corresponds to the tetrahedral clusters and the band near 450 cm^{-1} corresponds to the formation of octahedral clusters [11]. The vibrational mode of tetrahedral clusters is higher as compared to that of octahedral clusters because of the shorter bond length of Fe–O distance (0.189 nm) in the tetrahedral sites as compared to the Fe–O distance (0.199 nm) in the octahedral sites. It may be interpreted by the stronger bonding of Fe^{3+} ions at the A-sites than at the B-sites. The sharp peak ~720 cm^{-1} is due to the interference of nujol used as mulling agent.

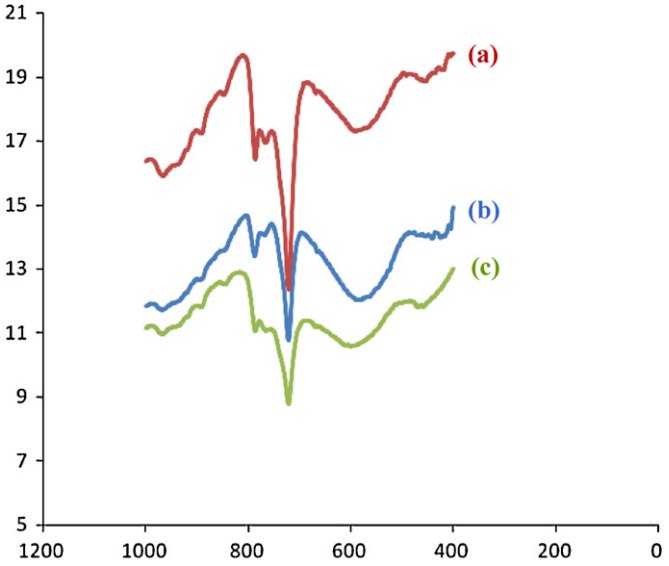

Fig. 1. FT-IR spectrum of $Co_{0.5}Zn_{0.5}Al_xFe_{2-x}O_4$ with (a) $x = 0.0$, (b) $x = 0.6$ and (c) $x = 1.0$ nanoferrites annealed at 1000 °C.

3.2. TEM analysis

The transmission electron microscope (TEM) images revealed that the particles of the as obtained samples are agglomerated and have spherical morphology with a particle size of ~100–300 nm, as reported in Singhal et al. [12]. This agglomeration may be attributed to the magnetic dipole interaction between the ferrite particles. However when the particles are agitated ultrasonically and taken on carbon grid, the particle size is observed to be ~10 nm, which increases with increasing annealing temperatures. It is believed that the net decrease in free energy of solid–solid and solid vapour interface provides the necessary driving force for the particle growth during annealing process [13]. Typical TEM images of $Co_{0.5}Zn_{0.5}Al_{0.6}Fe_{1.4}O_4$ annealed at 1000 °C are shown in

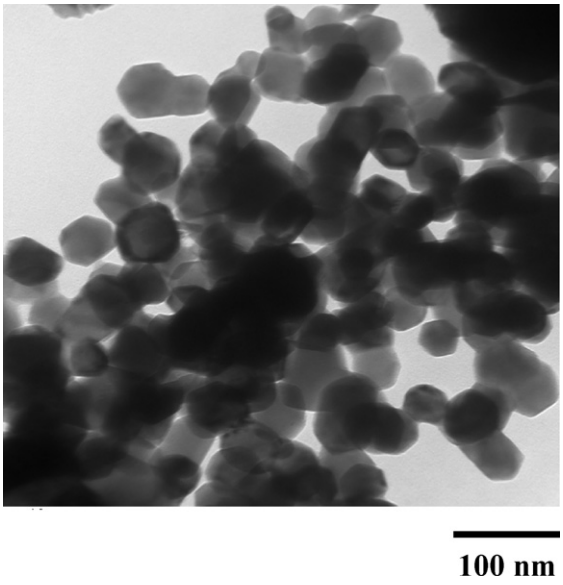

Fig. 2. TEM image of $Co_{0.5}Zn_{0.5}Al_{0.6}Fe_{1.4}O_4$ annealed at 1000 °C.

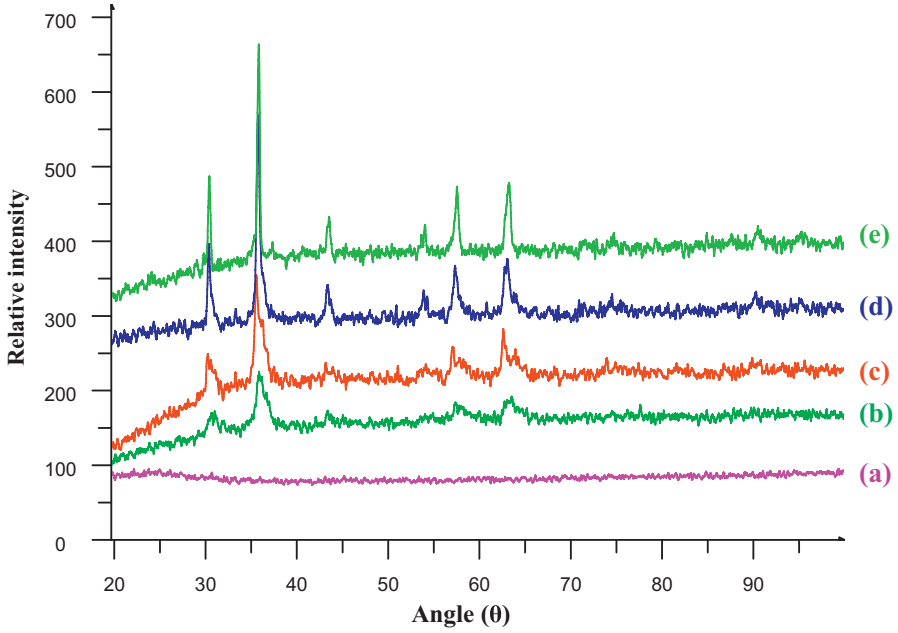

Fig. 3. Powder X-ray diffractographs of (a) as-obtained $Co_{0.5}Zn_{0.5}Al_{0.6}Fe_{1.4}O_4$ and annealed at (b) 400 °C, (c) 600 °C, (d) 800 °C and (e) 1000 °C.

Fig. 2, which indicate that the particles are spherical in shape and the estimated average particle size is ~45 nm. This confirms that the particle size increases from ~10 nm to ~45 nm as the annealing temperature is increased up to 1000 °C.

3.3. X-ray diffraction studies

A phase analysis has been done for confirming the formation of the spinel type cubic structure using X-ray powder diffractographs. Fig. 3 shows XRD patterns of as obtained $Co_{0.5}Zn_{0.5}Al_{0.6}Fe_{1.4}O_4$ nanoferrite samples and after annealing at 400, 600, 800 and 1000 °C. The as-obtained samples of $Co_{0.5}Zn_{0.5}Al_{0.6}Fe_{1.4}O_4$ are found to be of amorphous in nature with no peaks, however, as the annealing temperature increases from 400 to 1000 °C, the peaks grew sharper attributing to increase in particle size with increasing temperature. The crystallite size has been calculated using the Debye Scherrer equation [14]:

$$d = \frac{0.9\lambda}{(w - w_1)\cos\theta}$$

where d is the grain diameter, w is the half intensity widths of the relevant diffraction peak and w_1 is the instrumental broadening, λ is the X-ray wavelength and θ is the angle of diffraction. The crystallite size has been calculated, considering the most intense peak at (3 1 1) plane. The increase in particle size is observed with increasing annealing temperature in conformity with TEM studies. Fig. 4 represents the XRD pattern of $Co_{0.5}Zn_{0.5}Al_xFe_{2-x}O_4$ $(0 \leq x \leq 1.0)$ samples after annealing at 1000 °C. The peaks can be indexed to (2 2 0), (3 1 1), (4 0 0), (5 1 1) and (4 4 0) planes of the cubic unit cell, which correspond to the single phased spinel type cubic structure having space group Fd-3m.

The dimensional changes in the lattice parameter have been calculated using Powley and Le-Bail refinement methods. The lattice parameter increases with the substitution of Zn^{2+} ions with Co^{2+} ions, to accommodate the Zn^{2+} ion of relatively larger ionic radii (88 pm) as compared to that of Co^{2+} ion (83.8 pm). With further substitution of Fe^{3+} ions with Al^{3+} ions, the lattice parameter decreases attributing to the smaller ionic radii of Al^{3+} ion as compared to Fe^{3+} ion (Table 1).

3.4. Electrical properties

The conductance in ferrites can be explained on the basis of Verwey mechanism, which involves electron exchange between the ions of the same element present in more than one valence state, distributed randomly on equivalent lattice sites [15,16]. Ferrites structurally form cubic close packed oxygen lattice

Table 1
Lattice parameter, saturation magnetization and coercivity of all the annealed samples at 1000 °C.

S. no.	Sample	Saturation magnetization (emu/g)	Coercivity (Oe)	Lattice parameter (a) (Å)
1	$Co_{0.5}Zn_{0.5}Fe_2O_4$	64.33	42	8.41
2	$Co_{0.5}Zn_{0.5}Al_{0.2}Fe_{1.8}O_4$	53.83	31	8.37
3	$Co_{0.5}Zn_{0.5}Al_{0.6}Fe_{1.4}O_4$	26.34	44	8.32
4	$Co_{0.5}Zn_{0.5}Al_{0.8}Fe_{1.2}O_4$	19.28	66	8.30
5	$Co_{0.5}Zn_{0.5}AlFeO_4$	11.23	162	8.26

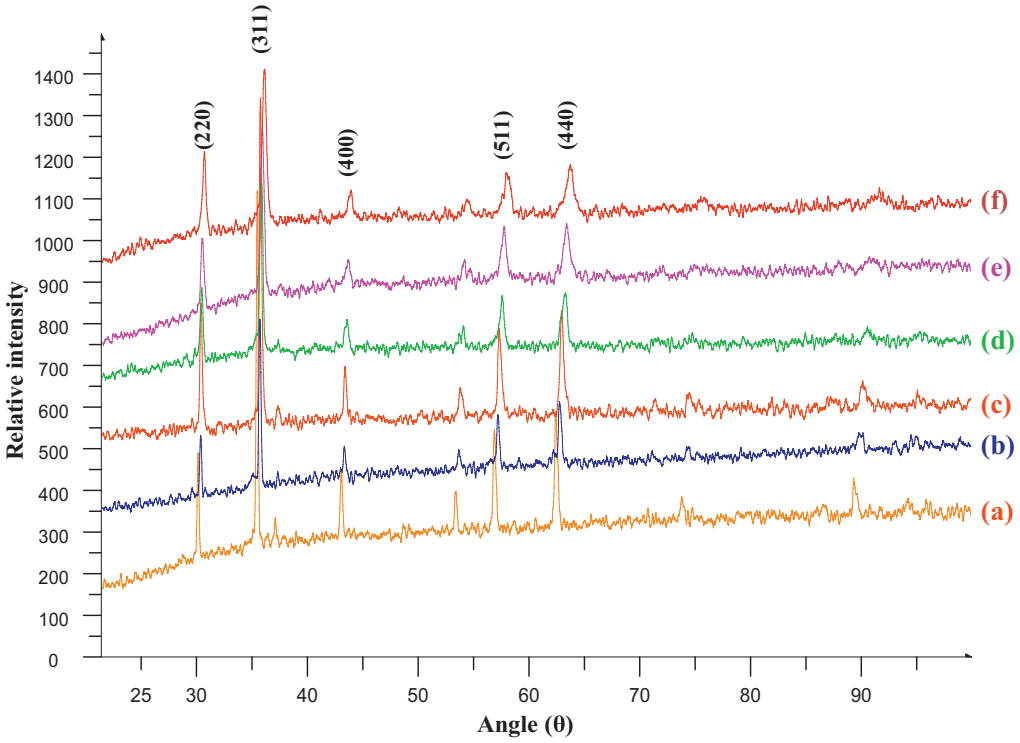

Fig. 4. Powder X-ray diffractographs of $Co_{0.5}Zn_{0.5}Al_xFe_{2-x}O_4 (0 \leq x \leq 1.0)$ with (a) $x = 0$, (b) $x = 0.2$, (c) $x = 0.4$, (d) $x = 0.6$, (e) $x = 0.8$ and (f) $x = 1.0$ annealed at 1000 °C.

with the metal cations in tetrahedral (A) sites and octahedral (B) sites. The distance between the metal cations in B sites is smaller as compared to their distance in A and B sites. This leads to greater probability of electron hopping between the cations in B–B sites than A–B hopping. The probability of hopping in A–A site is zero because of which A sites have only Fe^{3+} ions and Fe^{2+} ions formed occupies the B sites [17]. Therefore, the conduction in ferrites is due to the polaron hopping between Fe^{3+}–Fe^{2+} ions in the B sites.

Room temperature DC resistivity for all the samples with aluminium concentration is given in Table 2. It has been observed that the resistivity (ρ) increases from $\sim 2.3 \times 10^8$ ohm m to $\sim 3.55 \times 10^9$ ohm m, as the concentration of aluminium increases. This behavior of resistivity is attributed to the substitution of Fe^{3+} ions with Al^{3+} in B-sites [18]. The temperature dependency of DC resistivity in the temperature range 313–373 K, shows a decreasing resistivity with increasing the temperature, because the hopping rate increases with temperature. This leads to activation of the electrons to jump from Fe^{3+} to Fe^{2+} ions in the B sites, showing the semiconductor behavior [19,20]. The activation energy (E_a) has also been calculated using the Arrhenius type equation,

$$\rho = \rho_o \exp \frac{E_a}{kT}$$

where ρ_o is the resistivity at infinitely high temperature, k is the Boltzmann constant, E_a is the activation energy. The slope of (log ρ) versus ($1/kT$) gives the values of E_a values for all the samples as shown in Fig. 5. As the concentration of aluminium increases, the E_a decreases indicating the blocking of conduction mechanism between Fe^{3+} and Fe^{2+} ions due substitution of iron by aluminium in the B sites.

The decrease in DC resistivity with increasing temperature leads to increase in drift mobility (μ) of the charge carriers. This is due to the thermal activation of the charge carriers with increasing temperature. The drift mobility (μ) of the charge carriers has been calculated using the equation,

$$\mu = \frac{1}{ne\rho}$$

where e is the electronic charge, n is the number of charge carriers and ρ is the DC resistivity at temperature T. The variation of drift mobility versus resistivity at 313 K is shown in Fig. 8, which shows that the samples having high resistivity have low mobility and vice versa. An increasing trend of drift mobility with increasing temperature was observed (Fig. 6) due to the fact that the charge carriers start hopping from one site to

Table 2
Resistivity, activation energy and drift mobility of $Co_{0.5}Zn_{0.5}Al_xFe_{2-x}O_4$ ($0.0 \leq x \leq 1.0$) at 313 K.

x	Resistivity (ρ) $\times 10^9$ (ohm m)	Activation energy (E_a) (eV)	Drift mobility (μ) $\times 10^{-18}$ ($m^2\ v^{-1}\ s^{-1}$)
0.0	0.23	3.735	2.03
0.2	0.50	3.562	0.63
0.4	0.65	3.207	0.53
0.6	0.95	3.205	0.40
0.8	1.70	3.205	0.26
1.0	3.55	2.962	0.18

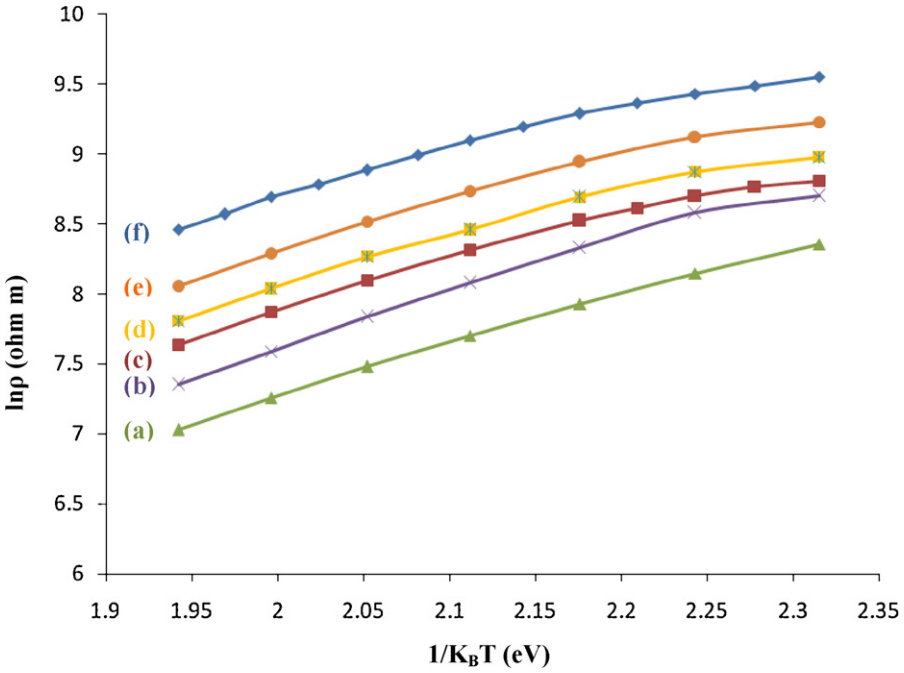

Fig. 5. Arrhenius plots of $Co_{0.5}Zn_{0.5}Al_xFe_{2-x}O_4$ ($0 = x = 1.0$) with (a) $x = 0$, (b) $x = 0.2$.

another with increasing temperature [21]. The various electrical parameters are tabulated in Table 2.

3.5. Magnetic measurements

Magnetic hysteresis loops at room temperature have been recorded for all the as obtained as well as annealed samples. Typical loops for $Co_{0.5}Zn_{0.5}Al_{0.6}Fe_{1.4}O_4$ after annealing at 400 and 1000 °C are shown in Fig. 7. It is observed in Fig. 7 that saturation magnetization increases with the annealing temperature due to the increase in particle size [22].

In a cubic system of ferromagnetic spinels, the magnetic order is mainly due to a super exchange interaction mechanism occurring between the metal ion in the A and B sublattices. The substitution of nonmagnetic ion such as zinc, which has a preferentially A site occupancy results in the reduction of the exchange interaction between A and B sites. Hence, by varying the degree of zinc substitution, it is possible to vary magnetic properties of the samples. Typical hysteresis loops of $Co_{0.5}Zn_{0.5}Al_xFe_{2-x}O_4$ ($x = 0$, 0.2, 0.6, 0.8 and 1.0) nanoferrites annealed at 1000 °C are shown in Fig. 8, which shows the effects of Al substitution on the magnetic properties of $Co_{0.5}Zn_{0.5}Fe_2O_4$ nanoferrites. The substitution of Al^{3+} ions for Fe^{3+} ions leads to a decrease in saturation magnetization. This may be attributed to the weakening of exchange interactions

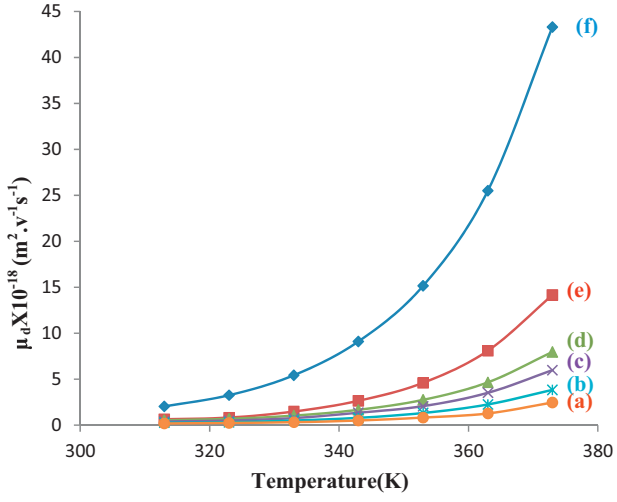

Fig. 6. Variation of drift mobility with temperature of $Co_{0.5}Zn_{0.5}Al_xFe_{2-x}O_4$ ($0 = x = 1.0$) with (a) $x = 0$, (b) $x = 0.2$, (c) $x = 0.4$, (d) $x = 0.6$, (e) $x = 0.8$ and (f) $x = 1.0$ annealed at 1000 °C.

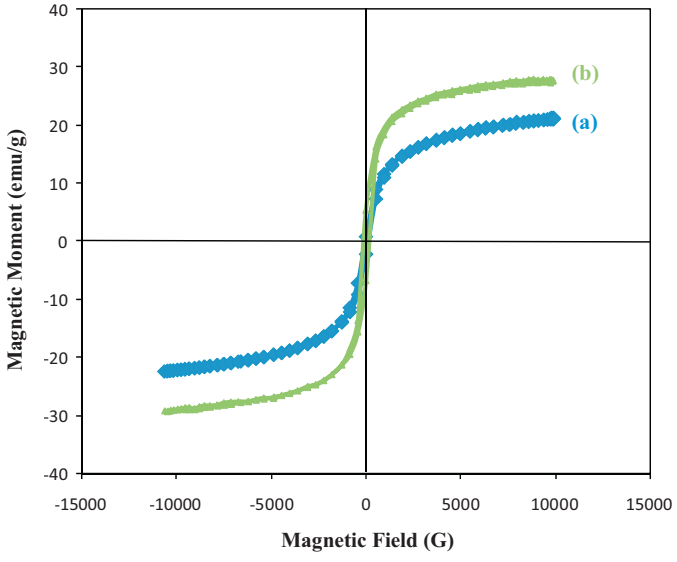

Fig. 7. Hysteresis loops of $Co_{0.5}Zn_{0.5}Al_{0.6}Fe_{1.4}O_4$ annealed at (a) 400 °C and (b) 1000 °C.

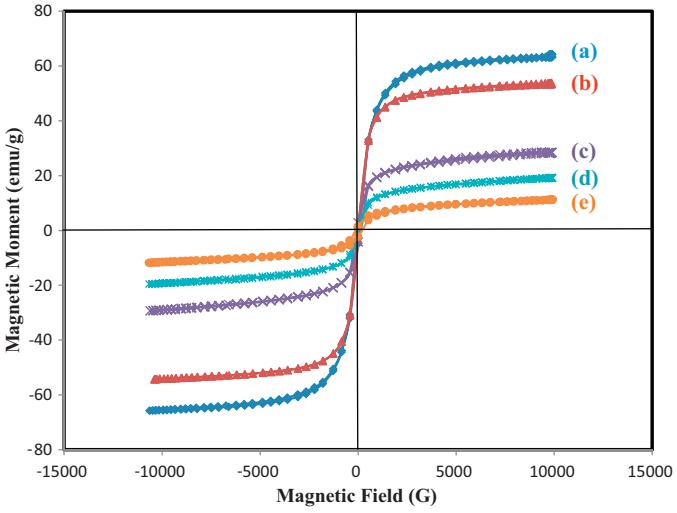

Fig. 8. Hysteresis loops of $Co_{0.5}Zn_{0.5}Al_xFe_{2-x}O_4$ ($0 = x = 1.0$) with (a) $x = 0$, (b) $x = 0.2$, (c) $x = 0.6$, (d) $x = 0.8$ and (e) $x = 1.0$ annealed at 1000 °C.

due to non magnetic Al^{3+} ions. An increase in coercivity with increasing aluminium concentration is observed which may be attributed to the increase in anisotropy field which in turn increases the domain wall energy [23–25].

4. Conclusion

Sol–gel auto-combustion method has been used to prepare $Co_{0.5}Zn_{0.5}Al_xFe_{2-x}O_4$ ($x = 0$, 0.2, 0.4, 0.6, 0.8 and 1.0) nanoferrites. Two fundamental peaks near $\sim$580 cm^{-1} and $\sim$450 cm^{-1} in the infrared spectrum confirmed the formation of M–O bonds in ferrites. XRD patterns reveal the single phase formation corresponding to the fcc cubical structure. The lattice parameter increases with zinc substitution but it decreases with aluminium substitution depending upon the sizes of ions substituted. The electrical resistivity increases with Al doping due to decrease in polaron hopping of Fe^{2+}–Fe^{3+} ions and the drift mobility increases with temperature due to their thermal activation. The drift mobility increases with increasing temperature due to hopping of the charge carriers from one site to another. There is a decrease in saturation magnetization value with zinc and aluminium ions substitution due to their diamagnetic nature whereas the coercivity value gets decreased with Zn^{2+} ion doping but increases with further substitution of Fe^{3+} ion with Al^{3+} ion.

Acknowledgement

Grateful thanks to the UGC for the financial support for this research work under the scheme of UGC-major project.

References

[1] S.R. Ahmed, P. Kofinas, Controlled room temperature synthesis of $CoFe_2O_4$ nanoparticles through a block co-polymer nanoreactor route, Macromolecules 35 (2002) 3338–3341.
[2] V.G Patil, S.E. Shirsath, S.D. More, S.J. Shukla, K.M. Jadhav, Effect of zinc substitution on structural and elastic properties of cobalt ferrite, J. Alloys Compd. 488 (2009) 199–203.
[3] R. Arulmurugan, B. Jeyadevan, G. Vaidyanathan, S. Sendhilnathan, Effect of zinc substitution on Co–Zn and Mn–Zn ferrite nanoparticles prepared by co-precipitation, J. Magn. Magn. Mater. 288 (2005) 470–477.
[4] G.V. Duong, N. Hanh, D.V. Linh, R. Groessinger, P. Weinberger, E. Schafler, M. Zehetbauer, Monodispersed nanocrystalline $Co_{1-x}Zn_xFe_2O_4$ O_4 particles by forced hydrolysis: synthesis and characterization, J. Magn. Magn. Mater. 311 (2007) 46–50.
[5] S.B. Waje, M. Hashim, W.D.W. Yousoff, Z. Abbas, Sintering temperature dependence of room temperature magnetic and dielectric properties of $Co_{0.5}Zn_{0.5}Fe_2O_4$ prepared using mechanically alloyed nanoparticles, J Magn. Magn. Mater. 322 (2010) 686–691.
[6] G. Vaidyanathan, S. Sendhilnathan, R. Arulmurgan, Structural and magnetic properties of $Co_{1-x}Zn_xFe_2O_4$ nanoparticles by co-precipitation method, J. Magn. Magn. Mater. 313 (2007) 293–299.
[7] S. Singhal, T. Namgyal, S. Bansal, K. Chandra, Effect of zinc substitution on the magnetic properties of cobalt ferrite nanoparticles prepared via sol–gel route, J. Electromagn. Anal. Appl. 2 (2010) 376–381.
[8] V.T. Thanki, K.H. Jani, B.S. Trivedi, K.B. Modi, H.H. Joshi, ^{57}Fe Mössbauer study on the spinel system $ZnxCo_{1-x}Fe_{2-x}Al_xO_4$, Mater. Lett. 37 (1998) 236–240.
[9] S.T. Alone, K.M. Jaghav, Structural and magnetic properties of zinc and aluminium substituted cobalt ferrite prepared by co-precipitation method, J. Phys. 70 (2008) 173–181.
[10] N.H. Vasoya, V.K. Lakhani, P.U. Sharma, K.B. Modi, R. Kumar, H.H. Joshi, Study on the electrical and dielectric behavior of Zn-substituted cobalt ferrialuminates, J. Phys.: Condens. Matter 18 (2006) 8063–8092.
[11] A. Pradeep, G. Chandrasekaran, FT-IR study of Ni, Cu and Zn substituted nanoparticles of $MgFe_2O_4$, Mater. Lett. 60 (2006) 371–374.
[12] S. Singhal, S.K. Barthwal, K. Chandra, Structural, magnetic and mössbauer spectral studies of nanosize aluminium substituted nickel zinc ferrite, J. Magn. Magn. Mater. 296 (2006) 94–103.
[13] A.C.F. Costa, E. Torella, M.R. Morelli, E.F. Neto, R.H.G.A. Kiminami, Sintering of Ni–Zn ferrite nanopowders by the constant heating rate (CHR) method, Mater. Res. 7 (2004) 523–528.
[14] H.P. Klug, L.E. Alexender, X-ray Diffraction Procedures for Polycrystalline and Amorphous Materials, 2nd ed., Wiley, 1974 (Chapter 9).
[15] E.J.W. Verwey, F. de Boer, J.H. van Santen, Cation arrangement in spinels, J. Chem. Phys. 16 (1948) 1091–1092.
[16] E.J.W. Verwey, P.W. Haayman, Electronic conductivity and transition point of magnetite ("Fe_3O_4"), Physica 8 (1941) 979–987.
[17] O.M Hameda, M.M. Barakat, Effect of hopping rate and jump length of hopping electrons on the conductivity and dielectric properties of Co–Cd ferrite, J. Magn. Magn. Mater. 223 (2001) 127–132.
[18] S.M. Ramay, S.A. Siddiqi, S. Atiq, M.S. Awan, S. Riaz, Structural, magnetic and electrical properties of Al^{3+} substituted Cu–Zn ferrites, Chin. J. Chem. Phys. 23 (2010) 591–595.
[19] M.J. Iqbal, M.R. Siddiquah, Structural, electrical and magnetic properties of Zr–Mg cobalt ferrite, Magn. Magn. Mater. 320 (2008) 845–850.
[20] M.A. Gabal, Y.M.A. Angari, Effect of diamagnetic substitution on the structural, magnetic and electrical properties of $NiFe_2O_4$, Mater. Chem. Phys. 115 (2009) 578–584.
[21] M.U. Islam, M.A. Chaudhry, T. Abbas, M. Umar, Temperature dependent electrical resistivity of Co–Zn–Fe–O system, Mater. Chem. Phys. 48 (1997) 227–229.
[22] A.H. Morrison, K. Haneda, Magnetic structure of small $NiFe_2O_4$ particles, J. Appl. Phys. 52 (1981) 2496–2498.
[23] B.D. Cullity, Introduction to Magnetic Materials, Addison-Wesely Publishing Company Inc., Reading, MA, 1972.
[24] S. Chikazumi, Physics of Magnetism, Wiley, New York, 1959.
[25] M. George, A.M. John, S.S. Nair, P.A. Joy, M.R. Anantharaman, Finite size effects on the structural and magnetic properties of sol-gel synthesized $NiFe_2O_4$ powders, J. Magn. Magn. Mater. 302 (2006) 190–195.